ACS Photonics

pubs.acs.org/journal/apchd5 Article

Deterministic Localization of Strain-Induced Single-Photon Emitters in Multilayer GaSe

Weijun Luo, Alexander A. Puretzky,* Benjamin J. Lawrie,* Qishuo Tan, Hongze Gao, Zhuofa Chen, Alexander V. Sergienko, Anna K. Swan, Liangbo Liang, and Xi Ling*

Cite This: https://doi.org/10.1021/acsphotonics.3c00052 Read Online

ABSTRACT: The nanoscale strain has emerged as a powerful tool for controlling single-photon emitters (SPEs) in atomically thin transition metal dichalcogenides (TMDCs). However, quantum emitters in monolayer TMDCs are typically unstable in ambient conditions. Multilayer TMDCs could be a solution, but they suffer from low quantum efficiency, resulting in low brightness of the SPEs. Here, we report the deterministic spatial localization of strain-induced SPEs in multilayer GaSe by nanopillar arrays. The strain-controlled quantum confinement effect introduces well-isolated sub-bandgap photoluminescence and corresponding suppression of the broad band edge photoluminescence. Clear photon-antibunching behavior is observed from the quantum dot-like GaSe sub-bandgap exciton emission at 3.5 K. The strain-dependent confinement potential and the brightness are found to be strongly correlated, suggesting a promising route for tuning and controlling SPEs. The comprehensive investigations of strain-engineered GaSe SPEs provide a solid foundation for the development of 2D devices for quantum photonic technologies.

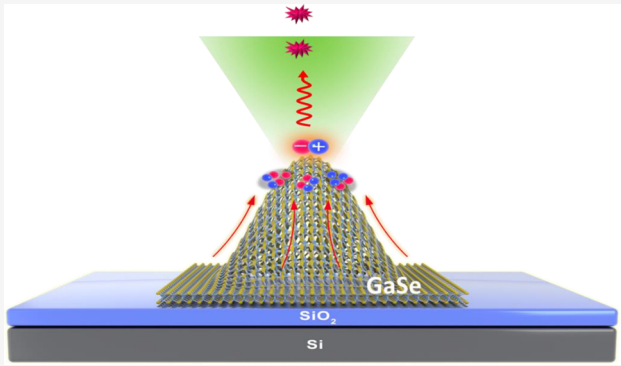

KEYWORDS: *2D materials, strain engineering, photoluminescence, gallium selenide*

■ INTRODUCTION

Over the past two decades, the scalable and controllable generation of SPEs with high brightness, purity, and indistinguishability has emerged as a critical requirement for developing photonic quantum technologies.[1,2] Recently, SPEs in 2D layered materials have drawn increasing interest because of the potential for deterministic generation and integrability with photonic devices.[3] SPEs arising from defect-bound excitons have been observed in monolayer TMDCs, such as WSe_2[4−6] with nanoscale strain providing deterministic control of SPEs.[7,8] Nevertheless, SPEs in monolayer TMDCs are sensitive to ambient instabilities that can cause a significant variation in the observed quantum optical properties.[8,9] On the other hand, multilayer TMDCs, which exhibit better stability, have indirect bandgaps and do not exhibit intense photoluminescence (PL).[10] As a result, research targeted at the control of SPEs in environmentally robust multilayer TMDCs has remained limited.

In contrast to the decreasing quantum yield of TMDCs with increasing numbers of layers, the band edge PL of layered GaSe increases dramatically with increasing numbers of layers,[11] suggesting that multilayer GaSe is a potential host for environmentally robust SPEs. Although multilayer GaSe has an indirect bandgap of 2.05 eV, there is a very small energy difference (<0.1 eV) between its indirect and direct bandgaps,[12,13] allowing for possible strain-induced indirect-to-direct bandgap transitions.[14] Prior PL studies of GaSe have shown that strain manipulation can significantly enhance its band edge PL emission by one order of magnitude.[15,16] However, reports of GaSe hosting SPEs are limited to the observations of randomly distributed SPEs that have been attributed to strain-bound excitons caused by inhomogeneous selenium clusters in the material.[17,18] To date, deterministic control of SPEs in multilayer GaSe with local strain has not been demonstrated.

In this study, we report an order-of-magnitude enhancement of the sub-bandgap PL emission from strained multilayer GaSe flakes (with thicknesses between 20 and 50 nm) on SiO_2 nanopillar arrays. Strong PL from strain-confined excitons and biexcitons with emission energies between 1.6 and 2.0 eV is observed at a temperature of T = 3.5 K. Notably, the exciton PL of GaSe at most pillar locations exhibits photon-antibunching characteristic of single-photon emission. By

Received: January 10, 2023

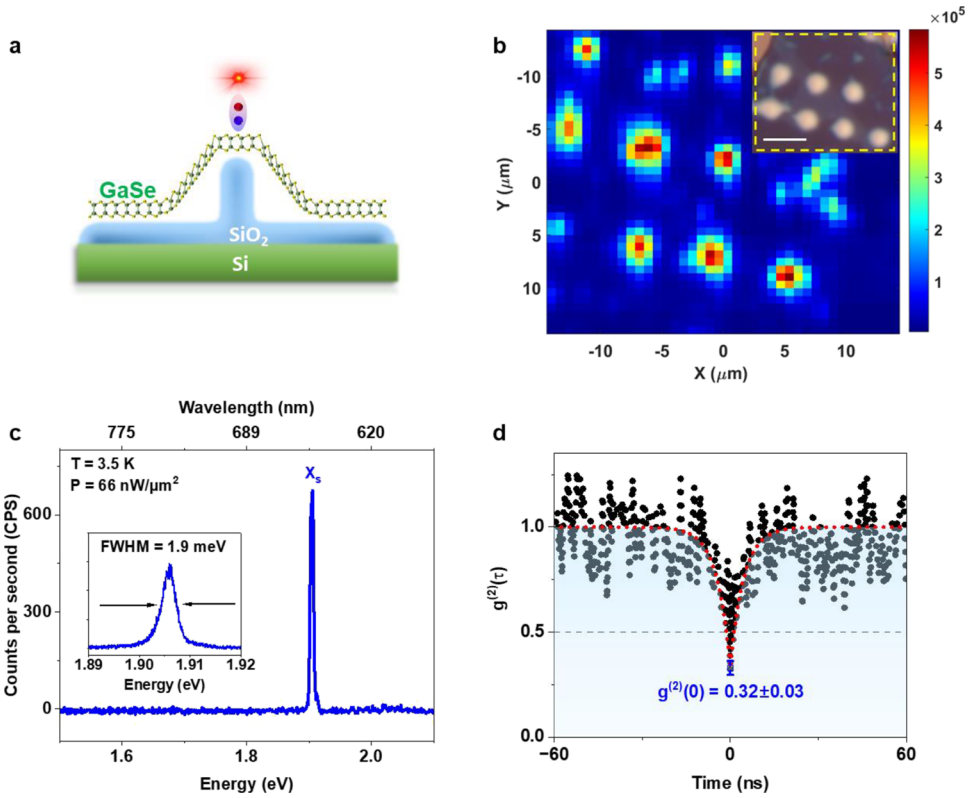

Figure 1. GaSe single photon emitters on nanopillar arrays. (a) Illustration of GaSe thin film tented on the pillar. For simplification, we used monolayer GaSe instead of multilayer GaSe in the illustration. (b) PL intensity map integrated across wavelengths of 600−800 nm for a representative array of pillars measured at T = 3.5 K, with an incident laser power density of 2 μW/μm^2. The inset optical image (scale bar, 5 μm) shows an exfoliated GaSe flake transferred onto SiO_2 nanopillar arrays. (c)Representative PL spectrum of GaSe on pillar apex with an incident laser power density of 66 nW/μm^2 measured at T = 3.5 K. The single photon emission is labeled as X_S. (d) Photon-antibunching measured for X_S acquired using a narrow band pass filter (650 nm, full width at half maximum (FWHM) = 10 nm) with an incident laser power density of 66 nW/μm^2 measured at T = 3.5 K. The fitted second-order correlation function shows $g^{(2)}(0)$ = 0.32 ± 0.02.

varying the incident laser power density, we show that the biexciton emission can be suppressed, resulting in improved single-photon purity. Moreover, the strain distribution around the pillar area is analyzed and used to quantify the effect of the strain-dependent quantum confinement on the emitter brightness with Pearson correlation analysis.[19] It clearly shows the positive correlation between strain, confinement potential, and brightness of the emitters. The control of confinement potential through localized strain in these nanopillar geometries thus provides a key tool for fundamental studies of SPE photophysics in multilayer GaSe and for the development of 2D quantum photonic devices.

■ RESULTS AND DISCUSSION

PL and Photon-Antibunching Characterization of Emitters in Multilayer GaSe. As shown in Figure 1a, multilayer GaSe flakes (with a thickness of ∼30 nm) are first mechanically exfoliated from high-quality ε-type GaSe bulk crystals (the crystal structure of a monolayer and Raman spectrum of GaSe bulk crystal are shown in Supplementary Figure S1) and then transferred to a Si substrate with pre-patterned SiO_2 nanopillar arrays (see more details on the sample preparation and pillar topography in Supplementary Figures S2 and S3, respectively). For simplification, we illustrate monolayer GaSe instead of multilayer GaSe in the schematic shown in Figure 1a. The SiO_2 nanopillar arrays were designed with three diameters of ∼150, ∼200, and ∼250 nm, and an average height of ∼100 nm (Supplementary Figure S4). The nanopillar diameters were chosen to be less than half of the excitation wavelength of 532 nm to drive quantum confinement effects.[20] The GaSe flake is tented uniformly on most pillars without piercing or breakage (as shown in the AFM image of Supplementary Figure S5). Since the PL intensity of GaSe increases drastically for thickness between 20 and 50 nm,[11] the thicknesses of all GaSe flakes studied here are within this range. Figure 1b shows an extracted PL intensity map (measured at T = 3.5 K with a laser power density of 2 μW/μm^2. The complete map of a prototypical GaSe flake (thickness, ∼30 nm) transferred onto a SiO_2 nanopillar array that is shown in Supplementary Figure S6, see also the inset). At this moderately high laser power density, several PL bands are observed spanning 600−750 nm (Supplementary Figure S7). The ratio of the strain localized GaSe PL to the band edge emission X_{E_g} is significantly enhanced by two orders of magnitude on the pillars. At a much lower laser power density of 44 nW/μm^2, PL spectra measured at T = 3.5 K on the pillars exhibited a few strong and well-separated features without the broad background or additional defect-related bands that are often observed in WSe_2[5] and hBN.[21,22] For example, in Figure 1c, the PL spectrum collected from GaSe on a pillar shows a single peak X_S at ∼1.90 eV (∼652 nm), about ∼0.15 eV below the well-studied GaSe band edge emission X_{E_g} at 2.05 eV.[23−26] Note that the emission energies of GaSe SPEs measured here are consistent with previous study on GaSe SPEs associated

https://doi.org/10.1021/acsphotonics.3c00052
ACS Photonics XXXX, XXX, XXX−XXX

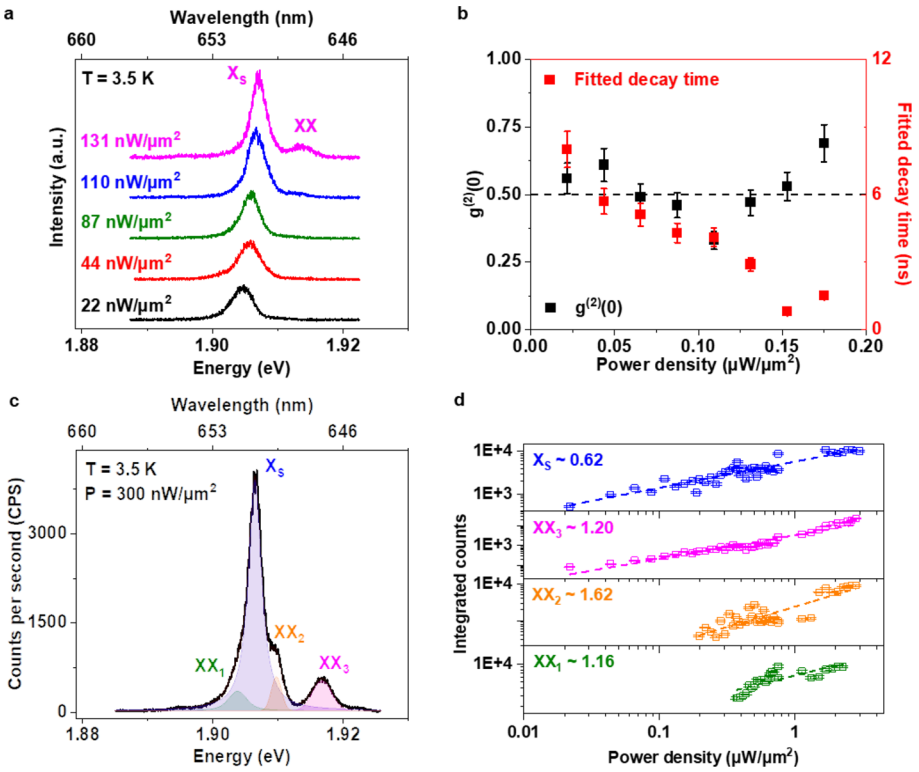

Figure 2. Power density-dependent PL spectra and photon-statistics measurements of the same GaSe SPE at ∼1.90 eV (∼652 nm) (shown in Figure 1c) acquired at T = 3.5 K. (a) Selected power density-dependent PL spectra of the SPE under relatively low excitation power density (<150 nW/μm^2). (b) Photon antibunching measurements of this SPE under different incident laser power densities. (c) Deconvolution of a PL spectrum of the SPE excited under a relatively high excitation power density of ∼300 nW/μm^2 that consists of three biexcitons (XX_1, XX_2, and XX_3) and one exciton (X_S) feature. (d)Integrated counts of the three biexcitons and the exciton as a function of incident laser power density.

with strain developed on GaSe film on randomly distributed selenium clusters.[17]

To evaluate the antibunching performance of this SPE, Hanbury Brown−Twiss (HBT) interferometry was used to characterize the second-order correlation function $g^{(2)}(\tau)$ of the emission peak X_S at ∼1.90 eV (∼652 nm). As shown in Figure 1d, antibunching with $g^{(2)}(0) = 0.32 \pm 0.02$, and a decay time-constant of ∼4.1 ± 0.7 ns is observed (the fitting details are discussed in Section 6 in the Supplementary Information). Overall, we investigated 97 emitters in total (as shown in Figure S8a), among them, 62 emitters have $g^{(2)}(0) < 0.5$, which are identified as SPEs; 35 emitters have $0.5 < g^{(2)}(0) < 1$, which are identified as non-SPEs. The $g^{(2)}(0)$ values of SPEs range from 0.2 to 0.5 (as shown in Figure S8b). The $g^{(2)}(0)$ values of non-SPEs range from 0.5 to 0.8 (as shown in Figure S8c). Also, the wavelengths of SPEs and non-SPEs that investigated match well with the results shown in Supplementary Figure S9. We also identify GaSe SPEs on the pillars with energies of 1.65−2.0 eV and time constants of 0.7−15.5 ns, as summarized in Supplementary Figures S10 and S11. However, the observed sub-bandgap transitions exhibit varying single-photon purity, as shown in Supplementary Figure S12, some emitters with $g^{(2)}(0) > 0.5$ are also observed. The GaSe SPEs exhibited an average wandering value of ∼0.5 nm under different incident laser power densities (Supplementary Figure S13). Note that the spectral wandering values, typically larger than 2 nm, were observed for WSe_2[5,27−31] and hBN[32−34] SPEs without any engineering. However, no significant blinking or bleaching is observed for all the SPEs studied. Moreover, our samples were kept in a glove box filled with inert gas (N_2/Ar) despite a few hours of exposure in the air due to transferring and loading. They did not experience obvious degradation (Supplementary Figure S14) like in the previous report.[35−38] After 18 months, the samples still exhibited strong emission intensities on the pillars (Supplementary Figure S15), and an SPE was characterized (Supplementary Figure S16).

Power-Dependent PL and Photon-Antibunching Characterization of a GaSe SPE. Note that the incident laser power density is critical in the single-photon purity. Previous studies of SPEs in quantum dots,[39] carbon nanotubes,[40] color centers in diamond,[41] and WSe_2[42] have demonstrated that a low excitation power density is required to minimize the emergence of additional excited states that can reduce the SPE purity. Power-dependent photon antibunching has been extensively investigated in WSe_2[30,43] and hBN[44,45] SPEs, but remains underexploited in GaSe SPEs. Therefore, to probe the interplay between brightness and purity for this 1.90 eV SPE, we performed PL and HBT interferometry measurements with various incident laser power densities. Figure 2a shows five high-resolution spectra collected with incident laser power densities from 22 to 131 nW/μm^2: a single symmetric exciton peak X_S (at ∼1.905 eV) is present at laser power densities below 87 nW/μm^2. A weaker biexciton peak XX (at ∼1.916 eV) emerges on the higher energy side of the excitonic peak X_S (energy shift $|\Delta E| \sim 11$ meV) and becomes relatively prominent for an incident laser power density of ∼131 nW/μm^2. Note that the biexciton formation with a binding energy of ∼2 meV was reported for GaSe.[46]

Figure 2b illustrates HBT interferometry measurement results as functions of incident laser power densities: $g^{(2)}(0)$

https://doi.org/10.1021/acsphotonics.3c00052
ACS Photonics XXXX, XXX, XXX−XXX

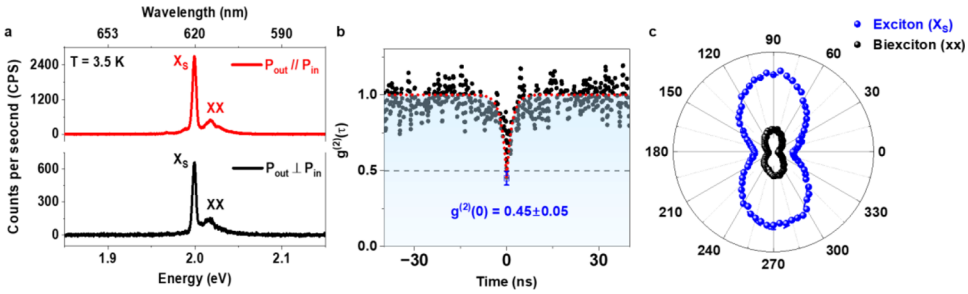

Figure 3. Characterization of a GaSe SPE at 1.99 eV (∼620 nm) with a horizontally polarized excitation at T = 3.5 K. The incident laser power density is 110 nW/μm^2 and a narrow band pass filter (622 nm, FWHM = 10 nm) is used for antibunching measurements. (a) Parallel- and cross-polarized PL spectra. (b) Second-order correlation function for the same SPE with the unpolarized collection. (c) Integrated polarization-dependent PL intensities from the exciton at 1.99 eV (∼620 nm) and biexciton at 2.02 eV (∼615 nm), respectively. The increment of measurement is 2.5°.

remains less than 0.5 when the incident laser power density is in the range of 60−130 nW/μm^2 (the photon-antibunching results obtained at different powers could be referred to Supplementary Figure S17a−h). With the increase of the laser power density, the $g^{(2)}(0)$ increases and the SPE purity reduces, due to the increased contribution of the biexciton that is too close to the exciton to be filtered by the narrow band pass filter. Also, continuously decreasing the power would not improve the $g^{(2)}(0)$. As inhomogeneous linewidth broadening caused by multiple complicated sources, such as electron−phonon coupling,[47,48] and defect-related non-radiative decay,[49−53] will play a significant role in the SPE quality, leading to the decrease of the $g^{(2)}(0)$. In addition to the power-dependent $g^{(2)}(0)$, we further performed the spectral weight analysis in Supplementary Figure S12i. The SPE spectra lineshapes are fitted by Voigt function ($V(x)$), which is the sum of Gaussian (inhomogeneous broadening) and Lorentzian (homogeneous broadening) functions: $V(x) \approx (1-\nu)L_1(x) + (\nu)G_1(x)$, where the spectral weight ν determines the overall lineshape, $G_1(x)$ and $L_1(x)$ are a Gaussian and a Lorentzian function, respectively. For SPE that follows an exact two-state transition, a Lorentzian lineshape is expected.

Supplementary Figure S17i shows that at the optimized power of 110 nW/μm^2, the spectral weight ν reaches a minimum, suggesting the largest probability of a two-state transition. Further lowering the excitation power will increase the ν, suggesting the Gaussian lineshape caused by inhomogeneous broadening becomes more significant.

Also, in Figure 2b, the decay time decreases with increasing excitation power could be explained by two different reasons: (1) For increasing excitation power up to 110 nW/μm^2, the increasing radiative efficiency of excitons results in the decreasing decay time and enhances the brightness of the emitter. (2) For increasing excitation power above 110 nW/μm^2, the exciton emission saturates, and the increasing emission intensities of biexciton lead to the decreasing decay time.

Hence, our results indicate that the brightness increase under a higher incident laser power density does not necessarily improve the SPE purity due to the emergence of the biexciton features. Consistent results were also observed on another SPE at ∼1.79 eV (693 nm), and the additional power density-dependent photon-antibunching measurements are shown in Supplementary Figures S18 and S19. Figure 2c illustrates a PL spectrum of the same emitter at 1.90 eV (652 nm) acquired with a higher incident laser power density of 300 nW/μm^2, where there is no observed antibunching. Four peaks are observed and labeled as XX_1, X_S, XX_2, and XX_3 at ∼1.904, ∼1.907, ∼1.910, and ∼1.916 eV, respectively. Note that previous studies demonstrated that the GaSe PL peaks could be classified into excitons[14] and biexcitons[46] according to the sub-linear and super-linear power-law scaling of the PL intensity. Figure 2d shows the integrated counts(C) of different peaks as a function of incident laser power densities (P) plotted in a double-logarithmic plot and fitted using the power-law function: $C \propto P^x$. The measured slope, x, can be used to classify GaSe excitons[17,54] and biexcitons[17,55] because excitons and biexcitons exhibit slopes of less than one and larger than one, respectively. The slope of the X_S peak is 0.62, so X_S is assigned to an exciton feature; XX_1, XX_2, and XX_3 have slopes greater than one, and they are identified as biexciton features.

Interestingly, some biexcitons (i.e., XX_1 and XX_2) are observed with higher energy than the exciton, implying negative binding energies. Across all the results, we observe both negative and positive biexciton binding energies (as summarized in Supplementary Figure S20). Negative biexciton binding energies resulting from biexciton antibonding or exciton−exciton repulsion have been primarily observed in quantum dot systems.[56−59] Hence, it could be inferred that the nanopillar arrays cause the formation of a quantum confinement potential, resulting in quantum dot-like GaSe SPEs. The localized strain in GaSe at different pillars introduces different confinement potential,[60] charge-carrier localization,[61] and charge separation,[62] leading to the different observed exciton and biexciton binding energies, as well as different required laser power densities for the formation of excitons.

Polarization-Dependent Characterization of Exciton and Biexciton in a GaSe SPE. Polarization-dependent measurements on an SPE and the corresponding biexciton are performed to better understand the relationship between the exciton and biexciton. Figure 3a shows the PL spectra of an emitter X_S (at 1.99 eV, ∼620 nm) acquired with a horizontally polarized excitation laser light in parallel- and cross-polarized collection configurations. The 2.02 eV (∼615 nm) peak was recognized as a biexciton feature from the power density-dependence measurements (Supplementary Figure S21b). In Figure 3b, the least squares fitting of the second-order correlation function produces the fitted value of $g^{(2)}(0)$ = 0.46 ± 0.03. Figure 3c illustrates the integrated polarization-dependent PL from both the exciton X_S and the biexciton XX. They share the same polarization response, suggesting that the exciton and biexciton share the same electric dipole transition that is linearly oriented in the quantum dot. Note that the co-

https://doi.org/10.1021/acsphotonics.3c00052
ACS Photonics XXXX, XXX, XXX−XXX

polarization of the exciton and biexciton that are close to each other and arising from the same emitter have been reported both in quantum dots[63] and 2D materials.[64] Thus, we assume that the exciton and the biexciton are both associated with the same quantum-dot-like emitter. For this SPE, laser power densities of less than 13 nW/μm^2 fully suppress the biexciton, as shown in Supplementary Figure S21a. Also, the additional polarization measurements on a couple of other emitters were conducted: for example, Figure S22 shows another emitter at 710 nm with one exciton at 1.746 eV (~710 nm) and one biexciton at 1.759 eV (~705 nm). The exciton and biexciton show co-polarization, suggesting that they originate from the same emitter.

Correlation Analysis of Strain and PL. To better understand the correlation between the strain-induced quantum confinement and the extraordinary enhancement of GaSe sub-bandgap emission (<2.05 eV), we analyze the localized strain distribution on individual pillars by measuring the height profiles of GaSe flakes on pillars with atomic force microscopy (AFM). Figure 4a shows an AFM image with a dimension of 3 μm × 3 μm, where a multilayer GaSe flake (~30-nm-thick) on a pillar with a diameter of ~200 nm formed a tent with a diameter of ~2 μm without any piercing. The classical Landau continuum model[65] for structural stress analysis (which has been commonly used to describe the nanoscale strain in nano-cubes,[7] nano-trenches,[66] and nano-bubbles[67]) is used to obtain the strain distribution across the pillar. More details about the strain simulation are shown in Supplementary Section 15 and Figure S23. Figure 4b illustrates the simulated position-dependent strain obtained from the AFM height profiles, as shown in Figure 4a. The resolution of the strain simulation is set to be ~700 nm (yielding an 8 × 8 strain matrix) so that it is slightly coarser than the PL mapping resolution of ~400 nm.

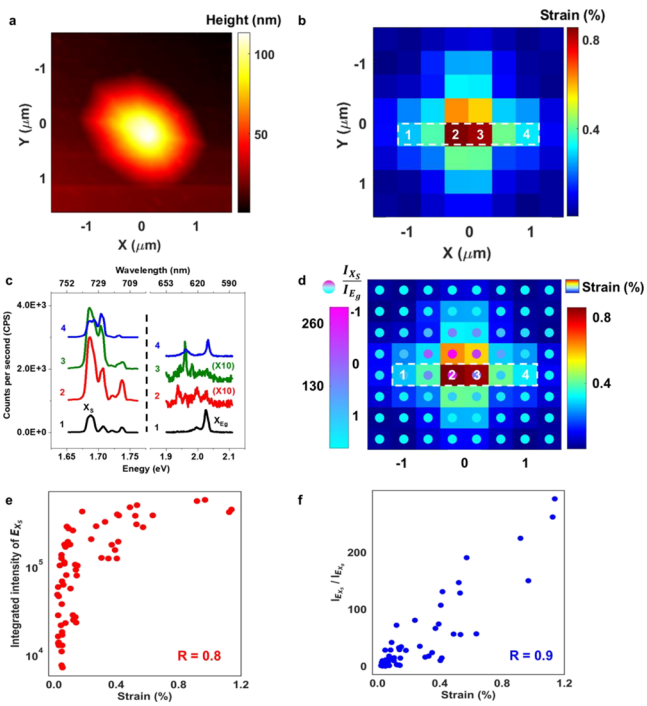

Figure 4. Correlation of strain distribution analysis with PL mapping results at T = 3.5 K. (a) AFM height profile of pillar 1 (marked in Supplementary Figures S5 and S6). (b) Strain map obtained from the AFM height profile in (a): each pixel covers an area of 0.7 μm ×0.7 μm, and the corresponding color represents the averaged strain (biaxial tensile strain). (c) Four PL spectra collected at the numbered positions, as shown in (b). (d) Correlation map of strain (squares, adapted from (b)) and the integrated PL intensity ratios (circles) between the sub-bandgap (strain-confined exciton) and band edge emission I_{X_S}/X_{E_g} plotted on a 5.6 × 5.6 μm grid. (e) Pearson correlation analysis of strain and the integrated sub-bandgap intensity I_{X_S}. (f) Pearson correlation analysis of strain and the integrated intensity ratios of $\frac{I_{X_S}}{I_{X_{E_g}}}$.

Figure 4c illustrates four representative PL spectra that are labeled in Figure 4b, where PL spectra 1 (black) and 4 (blue) are collected at the edge of the pillar dome (corresponding to the minimum strain). In contrast, PL spectra 2 (red) and 3 (green) are collected at the pillar apex (corresponding to the maximum strain). Well-defined band edge emission E_g at 2.02 eV (with relatively weak sub-bandgap emission X_S at 1.69 eV) is observed at sites 1 and 4. At sites 2 and 3, several sub-bandgap peaks appear at ~1.69 eV with brightness about two orders of magnitude larger than those in spectra 1 and 4. In contrast, the band edge emission X_{E_g} becomes much weaker. To specify, the peaks between 1.95 and 2.02 eV in PL spectra 2 (red) and 3 (green) arise from the indirect and direct excitons of GaSe.[13] Additional PL spectra from this pillar are shown in Supplementary Figure S24. A similar trend is also observed for other pillars, as shown in Supplementary Figures S25 and S26. In general, unlike the general co-presence of sub-bandgap and band edge emission on selenium clusters,[17] the sub-bandgap and band edge emissions on the pillar could be efficiently enhanced and suppressed, respectively.

Moreover, Figure 4d illustrates the position-dependent integrated PL intensity ratio ($\frac{I_{X_S}}{I_{X_{E_g}}}$) map together with the calculated strain at different locations: the ratio of the sub-bandgap emission to the band edge emission ($\frac{I_{X_S}}{I_{X_{E_g}}}$) is enhanced by roughly two orders of magnitude on the pillar compared to that on the bare substrate area. A Pearson correlation analysis of the strain and PL intensity ratio ($\frac{I_{X_S}}{I_{X_{E_g}}}$) provides a quantitative evaluation of their correlation strength. Note that Pearson correlation is a measure of the linear correlation between two sets of data that can be written as:

$$R = \frac{\sum (x_i - \underline{x})(y_i - \underline{y})}{\sqrt{(x_i - \underline{x})^2 (y_i - \underline{y})^2}}$$

where R is the Pearson correlation coefficient, x_i and y_i are two sets of data, and $\underline{x}$ and $\underline{y}$ are their mean values, respectively. A Pearson correlation coefficient larger than 0.7 suggests a strong positive correlation between the two sets of data.[19] This approach has been used to effectively interpret the linear correlation between two different features in PL spectroscopies of 2D semiconductors.[68−70] Figure 4e shows a strong positive Pearson correlation (R = 0.8) between the strain and the sub-bandgap emission intensities I_{X_S}. Figure 4f further shows a strong Pearson correlation (R = 0.9) between the stain and the PL intensity ratio ($\frac{I_{X_S}}{I_{X_{E_g}}}$). A two-order enhancement of I_{X_S} maps to a larger-than-0.2% biaxial tensile strain. However, $I_{X_{E_g}}$ has a weak negative correlation with the strain (R = −0.4) and I_{X_S} (R

https://doi.org/10.1021/acsphotonics.3c00052
ACS Photonics XXXX, XXX, XXX−XXX

= −0.45), and it vanishes when the biaxial tensile strain is larger than 0.2% (Supplementary Figure S26c,d). In addition, the strain and the redshift of sub-bandgap emission from the band edge also show a strong positive correlation (R = 0.731) (Supplementary Figure S27a,b).

Previous reports of the photoluminescence from strained GaSe[15,71,72] have shown significant enhancement of the band edge emission. Optical absorption easurements[71,73,74] under a backscattering configuration have revealed that the optical absorption coefficient of GaSe with light polarization perpendicular to the c axis ($\alpha_\perp$) is one order of magnitude larger than that parallel to the GaSe c axis ($\alpha\|$). Due to the tented structure of GaSe on the pillar, in the strained region, there is more contribution from $\alpha_\perp$ to the optical absorption, while in the unstrained region, the contribution from $\alpha_\perp$ is negligible. Increased optical absorption in the strained region could partially explain the extraordinary enhancement of sub-bandgap emission I_{X_S} (as shown in Figure 4e), but it does not explain the origin of the sub-bandgap emission I_{X_S} nor the attenuated band edge emission $I_{X_{E_g}}$. The red shift of the band gap due to the localized biaxial tensile strain might explain these observations. Therefore, we perform band structure calculation of biaxially strained bulk GaSe for a qualitative comparison via the density functional theory (DFT) approach. Despite the common underestimation of the bandgap by DFT, it still reflects the correct physical trend. Our results show a bandgap redshift rate of −0.18 eV/% under biaxial tensile strain (Supplementary Figure S28).

The DFT simulations also suggest that the valence band maximum and conduction band minimum show a blueshift rate of 0.086 eV/% and a redshift rate of −0.095 eV/%, respectively. This strain-induced opposing band bending behavior is defined as "Type-I funneling",[75] where the energy level of excited electrons descends towards the pillar apex with a larger strain while the energy level of holes ascends. As a result, the electrons and holes confined at the pillar apex have much higher concentrations than those at the flat region, which facilitates electron−hole recombination, leading to the enhancement of sub-bandgap emission and attenuation of band edge emission.

Additionally, to probe any potential antenna effects caused by the underlying pillar,[76] we performed a Mie scattering simulation on a SiO_2 nanopillar (Supplementary Figure S29a) and showed that no significant enhancement of Mie scattering would be introduced by the SiO_2 nanopillar (Supplementary Figure S29b).

CONCLUSIONS

In conclusion, we demonstrate the localization of quantum dot-like single-photon emitters in multilayer GaSe through strain control with SiO_2 nanopillar arrays. Ultimately, the results presented here provide a framework for stable, deterministic, and integrated quantum photonics. The GaSe SPEs arise from the exciton peak due to quantum confinement introduced by the localized nanoscale strain. The GaSe SPE purity is reduced with increasing excitation power density due to the formation of biexcitons. The incident laser power density required to excite an SPE varies at different sites due to the spatially varying confinement potentials. The local strain has a strong positive correlation with the sub-bandgap PL emission intensities and provides a two-order-of-magnitude enhancement in $\frac{I_{X_S}}{I_{X_{E_g}}}$. We attribute this increasing brightness of sub-bandgap emission to the strain-induced redshift of band gaps and the consequent "Type-I" exciton funneling. We envision that improved control over the localized charge concentration could help suppress biexciton PL and allow for bright, robust, and deterministic GaSe SPEs. We anticipate this demonstration of the deterministic localization of GaSe SPEs will stimulate future theoretical and experimental studies on SPEs in 2D materials and promote the development of quantum photonic devices and photonic quantum information technology.

METHODS

Synthesis of Bulk GaSe Crystal. Bulk GaSe was synthesized by the chemical vapor transport method.[77] A stoichiometric quantity of elements (molar ratio Ga:Se = 1:1, 1 g in total) and pure iodine (around 30 mg) were sealed into a quartz ampule under the pressure of <10^{-5} Pa. Then, the ampule was put in a two-zone furnace and kept at 820−870 °C, with the precursor side placed in the high-temperature zone, for a week. Van der Waals GaSe single crystals were collected from the low-temperature zone when the growth finished.

Fabrication of SiO_2 Nanopillar Arrays.

1. A 8 mm ×8 mm silicon chip (cut by a dicing saw) with a 300-nm-thick thermal oxide layer and alignment markers was spin-coated with PMMA photoresist (MicroChem 950 A3) at 2000 rpm for 45 s, and followed by a soft bake at 180 °C for 5 min.
2. The SiO_2 nanopillar arrays were patterned onto the chip by electron beam lithography via the Nanometer Pattern Generation System (NPGS) on a Zeiss Supra 40 scanning electron microscope. Then, the chip was developed in the isopropyl alcohol (IPA)/methyl isobutyl ketone (MIBK) mix solution (IPA:MIBK = 3:1) for 90 s, followed by a hard bake at 90 °C for 5 mins.
3. A 50-nm-chromium (Cr) protection layer was deposited (deposition rate: 0.5 Å/s) onto the chip via a CHA e-beam evaporator. Subsequently, a lift-off process in acetone was then performed to remove the Cr layer and keep only the developed region.
4. A reactive ion etching (RIE) process with fluoroform (CHF_3)/O_2 mixture gas was then performed on a Plasma-Therm 790 RIE etcher to etch a certain depth of SiO_2. A 9:1 (CHF_3)/O_2 and 40 Torr pressure would guarantee an etching rate of 70 nm/s on our machine.
5. After the RIE process, the residual Cr on the pillar was removed by immersing in the chromium etchant for 5 min. Then, the chip was rinsed with acetone, IPA, and DI water and treated with oxygen plasma to remove possible contaminants.

Transfer of GaSe Flake on SiO_2 Nanopillar Arrays. The GaSe flakes were first exfoliated onto a blank Si chip, and then a thin layer of poly-propylene carbonate (PPC) was spin-coated onto the chip. After curing at 60 °C for 5 min, the PPC layer carrying the GaSe flakes was detached from the chip and transferred onto the SiO_2 nanopillar arrays under the microscope.

Optical Spectroscopy. The cryo-PL and associated photon-statistics measurements were performed in a home-

https://doi.org/10.1021/acsphotonics.3c00052
ACS Photonics XXXX, XXX, XXX−XXX

built confocal PL microscope in a backscattering configuration. A Princeton Instruments Isoplane SCT-320 spectrograph with a Pixis 400BR Excelon camera and a grating turret with 150, 600, and 2400 g/mm gratings were used to measure PL spectra with the spectral resolutions of: ∼3.25 meV, ∼300 μeV, and ∼30 μeV, respectively. A 532 nm diode laser (Cobolt) was used for the excitation. A 100× in-vacuum objective (Zeiss, NA = 0.85) was integrated in the Montana S100 closed-cycle cryostat. The PL mapping was controlled by a 2-axis Galvo scanning.

Hanbury Brown−Twiss Interferometry. The photon-antibunching measurements by HBT experiments were carried out by utilizing a pair of large-area superconducting nanowire single-photon detectors (SNSPDs, Quantum Opus) and a Picoquant Hydraharp time-correlated single-photon counting (TCSPC) system. A 90:10 non-polarizing beam splitter was used to allow for PL (10% coupling efficiency) and photon correlation functions (90% coupling efficiency) to be acquired in parallel. Note that to show the explicit certification of the photon-antibunching dip at $\tau \rightarrow 0$,[78,79] the margin of x-axis (time delay) was set at least three times larger than the corresponding decay time of SPE.

DFT Simulations. Plane-wave DFT calculations were carried out using the Vienna Ab initio Simulation Package[28,29] (VASP) with projector augmented wave pseudopotentials[28,30,31] for electron-ion interactions, and the generalized gradient approximation functional of Perdew, Burke and Ernzerhof[80] for exchange-correlation interactions. Based on the bulk GaSe structure (Materials project database[81]), the strain-free and biaxial-strained GaSe cell were optimized with a cutoff energy of 350 eV and 12 × 12 × 2 k-point samplings until the maximum force allowed on each atom was less than 0.001 eV/Å. The total volume of the structure was fixed during geometry optimization to avoid the structural collapse of the 2D slabs with vacuum separations. The post-analysis of electronic band structures was carried out by using the VASPKIT package.[82]

■ ASSOCIATED CONTENT

Supporting Information

The Supporting Information is available free of charge at https://pubs.acs.org/doi/10.1021/acsphotonics.3c00052.

Description of methods; extended statistical PL and photon-antibunching characterization data for SPEs; photostability characterization; extended power-dependent PL and evaluation of single-photon purity; statistical analysis of exciton binding energies; strain simulation; extended correlation analysis of PL characterizations; DFT simulation results of strained GaSe;Mie scattering simulation (PDF)

■ AUTHOR INFORMATION

Corresponding Authors

Alexander A. Puretzky − *Center for Nanophase Materials Sciences, Oak Ridge National Laboratory, Oak Ridge, Tennessee 37831, United States;* orcid.org/0000-0002-9996-4429; Email: puretzkya@ornl.gov

Benjamin J. Lawrie − *Center for Nanophase Materials Sciences and Materials Science and Technology Division, Oak Ridge National Laboratory, Oak Ridge, Tennessee 37831, United States;* orcid.org/0000-0003-1431-066X; Email: lawriebj@ornl.gov

Xi Ling − *Department of Chemistry, Division of Materials Science and Engineering, and The Photonics Center, Boston University, Boston, Massachusetts 02215, United States;* orcid.org/0000-0003-3462-9088; Email: xiling@bu.edu

Authors

Weijun Luo − *Department of Chemistry, Boston University, Boston, Massachusetts 02215, United States*

Qishuo Tan − *Department of Chemistry, Boston University, Boston, Massachusetts 02215, United States;* orcid.org/0000-0002-5829-9119

Hongze Gao − *Department of Chemistry, Boston University, Boston, Massachusetts 02215, United States*

Zhuofa Chen − *Department of Electrical Engineering, Boston University, Boston, Massachusetts 02215, United States;* orcid.org/0000-0002-0331-1926

Alexander V. Sergienko − *Department of Electrical Engineering and The Photonics Center, Boston University, Boston, Massachusetts 02215, United States*

Anna K. Swan − *Department of Electrical Engineering and The Photonics Center, Boston University, Boston, Massachusetts 02215, United States;* orcid.org/0000-0002-3978-7993

Liangbo Liang − *Center for Nanophase Materials Sciences, Oak Ridge National Laboratory, Oak Ridge, Tennessee 37831, United States*

Complete contact information is available at: https://pubs.acs.org/10.1021/acsphotonics.3c00052

Author Contributions

W.L. and X.L. conceived the experiment. W.L. prepared the samples with assistance from Q.T., H.G., and Z.C. Q.T. synthesized and characterized the bulk GaSe crystals. W.L. conducted the PL and photon-statistics measurements with assistance from A.P. and B.L. at the Center for Nanophase Materials Sciences, Oak Ridge National Laboratory. W.L. performed theoretical calculations with assistance from L.L. W.L. performed the analysis and interpretation of the data with assistance from A.P., B.L., L.L., A.S., A.K.S., and X.L. All authors contributed to the writing of the manuscript.

Funding

This material is based upon study supported by the National Science Foundation (NSF) under Grant No. (1945364). Study by X.L. was supported by the U.S. Department of Energy (DOE), Office of Science, Basic Energy Sciences (BES) under Award DE-SC0021064. W.L., X.L., and A.K.S. acknowledge the support of National Science Foundation (NSF) under Grant No. (2111160). The photoluminescence and photon-statistics measurements were performed at the Center for Nanophase Materials Sciences (CNMS), which is a US Department of Energy Office of Science User Facility. W.L. acknowledges Dr. Y.Y. Pai from Oak Ridge National Laboratory for his help with experimental automation. X.L., A.S., and A.K.S. acknowledge the membership of the Photonics Center at Boston University. The computational study is performed using Shared Computing Cluster at Boston University.

Notes

The authors declare no competing financial interest.

REFERENCES

(1) Aharonovich, I.; Englund, D.; Toth, M. Solid-State Single-Photon Emitters. *Nat. Photonics* **2016**, *10*, 631.

(2) Eisaman, M. D.; Fan, J.; Migdall, A.; Polyakov, S. V. Invited Review Article: Single-Photon Sources and Detectors. *Rev. Sci. Instrum.* **2011**, *82*, No. 071101.

(3) Liu, X.; Hersam, M. C. 2D Materials for Quantum Information Science. *Nat. Rev. Mater.* **2019**, *4*, 669−684.

(4) Koperski, M.; Nogajewski, K.; Arora, A.; Cherkez, V.; Mallet, P.; Veuillen, J.-Y.; Marcus, J.; Kossacki, P.; Potemski, M. Single Photon Emitters in Exfoliated WSe 2 Structures. *Nat. Nanotechnol.* **2015**, *10*, 503.

(5) He, Y.-M.; Clark, G.; Schaibley, J. R.; He, Y.; Chen, M.-C.; Wei, Y.-J.; Ding, X.; Zhang, Q.; Yao, W.; Xu, X.; Lu, C.-Y.; Pan, J.-W. Single Quantum Emitters in Monolayer Semiconductors. *Nat. Nanotechnol.* **2015**, *10*, 497−502.

(6) Tran, T. T.; Bray, K.; Ford, M. J.; Toth, M.; Aharonovich, I. Quantum Emission from Hexagonal Boron Nitride Monolayers. *Nat. Nanotechnol.* **2016**, *11*, 37.

(7) Luo, Y.; Shepard, G. D.; Ardelean, J. V.; Rhodes, D. A.; Kim, B.; Barmak, K.; Hone, J. C.; Strauf, S. Deterministic Coupling of Site-Controlled Quantum Emitters in Monolayer WSe 2 to Plasmonic Nanocavities. *Nat. Nanotechnol.* **2018**, *13*, 1137.

(8) Parto, K.; Azzam, S. I.; Banerjee, K.; Moody, G. Defect and Strain Engineering of Monolayer WSe2 Enables Site-Controlled Single-Photon Emission up to 150 K. *Nat. Commun.* **2021**, *12*, 3585.

(9) Kumar, S.; Kaczmarczyk, A.; Gerardot, B. D. Strain-Induced Spatial and Spectral Isolation of Quantum Emitters in Mono-and Bilayer WSe2. *Nano Lett.* **2015**, *15*, 7567−7573.

(10) Mak, K. F.; Lee, C.; Hone, J.; Shan, J.; Heinz, T. F. Atomically Thin MoS 2: A New Direct-Gap Semiconductor. *Phys. Rev. Lett.* **2010**, *105*, No. 136805.

(11) Del Pozo-Zamudio, O.; Schwarz, S.; Sich, M.; Akimov, I. A.; Bayer, M.; Schofield, R. C.; Chekhovich, E. A.; Robinson, B. J.; Kay, N. D.; Kolosov, O. V.; et al. Photoluminescence of Two-Dimensional GaTe and GaSe Films. *2D Mater.* **2015**, *2*, No. 035010.

(12) Olguín, D.; Rubio-Ponce, A.; Cantarero, A. Ab Initio Electronic Band Structure Study of III−VI Layered Semiconductors. *Eur. Phys. J. B* **2013**, *86*, 350.

(13) Capozzi, V. Direct and Indirect Excitonic Emission in GaSe. *Phys. Rev. B* **1981**, *23*, 836.

(14) Ma, Y.; Dai, Y.; Guo, M.; Yu, L.; Huang, B. Tunable Electronic and Dielectric Behavior of GaS and GaSe Monolayers. *Phys. Chem. Chem. Phys.* **2013**, *15*, 7098−7105.

(15) Zhang, D.; Jia, T.; Dong, R.; Chen, D. Temperature-Dependent Photoluminescence Emission from Unstrained and Strained GaSe Nanosheets. *Materials* **2017**, *10*, 1282.

(16) Wang, C.; Yang, S.; Cai, H.; Ataca, C.; Chen, H.; Zhang, X.; Xu, J.; Chen, B.; Wu, K.; Zhang, H.; Liu, L.; Li, J.; Grossman, J. C.; Tongay, S.; Liu, Q. Enhancing Light Emission Efficiency without Color Change in Post-Transition Metal Chalcogenides. *Nanoscale* **2016**, *8*, 5820−5825.

(17) Tonndorf, P.; Schwarz, S.; Kern, J.; Niehues, I.; Del Pozo-Zamudio, O.; Dmitriev, A. I.; Bakhtinov, A. P.; Borisenko, D. N.; Kolesnikov, N. N.; Tartakovskii, A. I. Single-Photon Emitters in GaSe. *2D Mater.* **2017**, *4*, No. 021010.

(18) Tonndorf, P.; Del Pozo-Zamudio, O.; Gruhler, N.; Kern, J.; Schmidt, R.; Dmitriev, A. I.; Bakhtinov, A. P.; Tartakovskii, A. I.; Pernice, W.; Michaelis de Vasconcellos, S. On-Chip Waveguide Coupling of a Layered Semiconductor Single-Photon Source. *Nano Lett.* **2017**, *17*, 5446−5451.

(19) Moore, D. S.; Kirkland, S. *The Basic Practice of Statistics*; WH Freeman: New York, 2007; Vol. 2.

(20) Palacios-Berraquero, C.; Kara, D. M.; Montblanch, A. R.-P.; Barbone, M.; Latawiec, P.; Yoon, D.; Ott, A. K.; Loncar, M.; Ferrari, A. C.; Atatüre, M. Large-Scale Quantum-Emitter Arrays in Atomically Thin Semiconductors. *Nat. Commun.* **2017**, *8*, 15093.

(21) Feldman, M. A.; Puretzky, A.; Lindsay, L.; Tucker, E.; Briggs, D. P.; Evans, P. G.; Haglund, R. F.; Lawrie, B. J. Phonon-Induced Multicolor Correlations in HBN Single-Photon Emitters. *Phys. Rev. B* **2019**, *99*, No. 020101.

(22) Feldman, M. A.; Marvinney, C. E.; Puretzky, A. A.; Lawrie, B. J. Evidence of Photochromism in a Hexagonal Boron Nitride Single-Photon Emitter. *Optica* **2021**, *8*, 1−5.

(23) Besson, J. M.; Jain, K. P.; Kuhn, A. Optical Absorption Edge in GaSe under Hydrostatic Pressure. *Phys. Rev. Lett.* **1974**, *32*, 936.

(24) Capozzi, V.; Montagna, M. Optical Spectroscopy of Extrinsic Recombinations in Gallium Selenide. *Phys. Rev. B* **1989**, *40*, 3182.

(25) Capozzi, V.; Caneppele, S.; Montagna, M.; Levy, F. Radiative Decay from Free and Bound Excitons in GaSe. *Phys. Status Solidi B* **1985**, *129*, 247−257.

(26) Capozzi, V.; Caneppele, S.; Montagna, M. Luminescence of Selective Optical Pumping of Excitons in GaSe. *J. Lumin.* **1984**, *31*−*32*, 463−465.

(27) Daveau, R. S.; Vandekerckhove, T.; Mukherjee, A.; Wang, Z.; Shan, J.; Mak, K. F.; Vamivakas, A. N.; Fuchs, G. D. Spectral and Spatial Isolation of Single Tungsten Diselenide Quantum Emitters Using Hexagonal Boron Nitride Wrinkles. *APL Photonics* **2020**, *5*, No. 096105.

(28) Koperski, M.; Nogajewski, K.; Arora, A.; Cherkez, V.; Mallet, P.; Veuillen, J.-Y.; Marcus, J.; Kossacki, P.; Potemski, M. Single Photon Emitters in Exfoliated WSe2 Structures. *Nat. Nanotechnol.* **2015**, *10*, 503−506.

(29) Chakraborty, C.; Kinnischtzke, L.; Goodfellow, K. M.; Beams, R.; Vamivakas, A. N. Voltage-Controlled Quantum Light from an Atomically Thin Semiconductor. *Nat. Nanotechnol.* **2015**, *10*, 507.

(30) Srivastava, A.; Sidler, M.; Allain, A. V.; Lembke, D. S.; Kis, A.; Imamoğlu, A. Optically Active Quantum Dots in Monolayer WSe2. *Nat. Nanotechnol.* **2015**, *10*, 491−496.

(31) Tonndorf, P.; Schmidt, R.; Schneider, R.; Kern, J.; Buscema, M.; Steele, G. A.; Castellanos-Gomez, A.; van der Zant, H. S. J.; de Vasconcellos, S. M.; Bratschitsch, R. Single-Photon Emission from Localized Excitons in an Atomically Thin Semiconductor. *Optica* **2015**, *2*, 347−352.

(32) Li, X.; Shepard, G. D.; Cupo, A.; Camporeale, N.; Shayan, K.; Luo, Y.; Meunier, V.; Strauf, S. Nonmagnetic Quantum Emitters in Boron Nitride with Ultranarrow and Sideband-Free Emission Spectra. *ACS Nano* **2017**, *11*, 6652−6660.

(33) Elshaari, A. W.; Skalli, A.; Gyger, S.; Nurizzo, M.; Schweickert, L.; Esmaeil Zadeh, I.; Svedendahl, M.; Steinhauer, S.; Zwiller, V. Deterministic Integration of HBN Emitter in Silicon Nitride Photonic Waveguide. *Adv. Quantum Technol.* **2021**, *4*, No. 2100032.

(34) White, S. J.; Yang, T.; Dontschuk, N.; Li, C.; Xu, Z.-Q.; Kianinia, M.; Stacey, A.; Toth, M.; Aharonovich, I. Electrical Control of Quantum Emitters in a Van Der Waals Heterostructure. *Light: Sci. Appl.* **2022**, *11*, 186.

(35) Bergeron, A.; Ibrahim, J.; Leonelli, R.; Francoeur, S. Oxidation Dynamics of Ultrathin GaSe Probed through Raman Spectroscopy. *Appl. Phys. Lett.* **2017**, *110*, 241901.

(36) Beechem, T. E.; Kowalski, B. M.; Brumbach, M. T.; McDonald, A. E.; Spataru, C. D.; Howell, S. W.; Ohta, T.; Pask, J. A.; Kalugin, N. G. Oxidation of Ultrathin GaSe. *Appl. Phys. Lett.* **2015**, *107*, 173103.

(37) Rahaman, M.; Rodriguez, R. D.; Monecke, M.; Lopez-Rivera, S. A.; Zahn, D. R. GaSe Oxidation in Air: From Bulk to Monolayers. *Semicond. Sci. Technol.* **2017**, *32*, 105004.

(38) Shi, L.; Li, Q.; Ouyang, Y.; Wang, J. Effect of Illumination and Se Vacancies on Fast Oxidation of Ultrathin Gallium Selenide. *Nanoscale* **2018**, *10*, 12180−12186.

(39) Kimura, S.; Kumano, H.; Endo, M.; Suemune, I.; Yokoi, T.; Sasakura, H.; Adachi, S.; Muto, S.; Song, H. Z.; Hirose, S.; Usuki, T. Photon Antibunching Observed from an InAlAs Single Quantum Dot. *Jpn. J. Appl. Phys.* **2005**, *44*, L793.

(40) Högele, A.; Galland, C.; Winger, M.; Imamoğlu, A. Photon Antibunching in the Photoluminescence Spectra of a Single Carbon Nanotube. *Phys. Rev. Lett.* **2008**, *100*, No. 217401.

(41) Beveratos, A.; Brouri, R.; Poizat, J.-P.; Grangier, P. Bunching and Antibunching from Single NV Color Centers in Diamond. In

https://doi.org/10.1021/acsphotonics.3c00052
ACS Photonics XXXX, XXX, XXX−XXX

Quantum Communication, Computing, and Measurement 3; Springer, 2002; pp 261−267.
(42) Gao, T.; von Helversen, M.; Anton-Solanas, C.; Schneider, C.; Heindel, T. Atomically-Thin Single-Photon Sources for Quantum Communication. *npj 2D Mater. Appl.* **2023**, *7*, 4.
(43) Chen, X.; Lu, X.; Dubey, S.; Yao, Q.; Liu, S.; Wang, X.; Xiong, Q.; Zhang, L.; Srivastava, A. Entanglement of Single-Photons and Chiral Phonons in Atomically Thin WSe2. *Nat. Phys.* **2019**, *15*, 221−227.
(44) Vogl, T.; Campbell, G.; Buchler, B. C.; Lu, Y.; Lam, P. K. Fabrication and Deterministic Transfer of High-Quality Quantum Emitters in Hexagonal Boron Nitride. *ACS Photonics* **2018**, *5*, 2305−2312.
(45) Schell, A. W.; Svedendahl, M.; Quidant, R. Quantum Emitters in Hexagonal Boron Nitride Have Spectrally Tunable Quantum Efficiency. *Adv. Mater.* **2018**, *30*, No. 1704237. e1704237
(46) Dey, P.; Paul, J.; Moody, G.; Stevens, C. E.; Glikin, N.; Kovalyuk, Z. D.; Kudrynskyi, Z. R.; Romero, A. H.; Cantarero, A.; Hilton, D. J.; Karaiskaj, D. Biexciton Formation and Exciton Coherent Coupling in Layered GaSe. *J. Chem. Phys.* **2015**, *142*, 212422.
(47) Grosso, G.; Moon, H.; Ciccarino, C. J.; Flick, J.; Mendelson, N.; Mennel, L.; Toth, M.; Aharonovich, I.; Narang, P.; Englund, D. R. Low-Temperature Electron−Phonon Interaction of Quantum Emitters in Hexagonal Boron Nitride. *ACS Photonics* **2020**, *7*, 1410−1417.
(48) Ripin, A.; Peng, R.; Zhang, X.; Chakravarthi, S.; He, M.; Xu, X.; Fu, K.-M.; Cao, T.; Li, M. Tunable Phononic Coupling in Excitonic Quantum Emitters. *Nat. Nanotechnol.* **2023**, 6.
(49) Neu, E.; Steinmetz, D.; Riedrich-Möller, J.; Gsell, S.; Fischer, M.; Schreck, M.; Becher, C. Single Photon Emission from Silicon-Vacancy Colour Centres in Chemical Vapour Deposition Nano-Diamonds on Iridium. *New J. Phys.* **2011**, *13*, No. 025012.
(50) Berhane, A. M.; Jeong, K.-Y.; Bradac, C.; Walsh, M.; Englund, D.; Toth, M.; Aharonovich, I. Photophysics of GaN Single-Photon Emitters in the Visible Spectral Range. *Phys. Rev. B* **2018**, *97*, No. 165202.
(51) Fishman, R. E.; Patel, R. N.; Hopper, D. A.; Huang, T.-Y.; Bassett, L. C. Photon-Emission-Correlation Spectroscopy as an Analytical Tool for Solid-State Quantum Defects. *PRX Quantum* **2023**, *4*, No. 010202.
(52) Castelletto, S.; Johnson, B. C.; Ivády, V.; Stavrias, N.; Umeda, T.; Gali, A.; Ohshima, T. A Silicon Carbide Room-Temperature Single-Photon Source. *Nat. Mater.* **2014**, *13*, 151.
(53) Luo, Y.; Liu, N.; Li, X.; Hone, J. C.; Strauf, S. Single Photon Emission in WSe_2 up 160 K by Quantum Yield Control. *2D Mater.* **2019**, *6*, No. 035017.
(54) Schwarz, S.; Dufferwiel, S.; Walker, P. M.; Withers, F.; Trichet, A. A. P.; Sich, M.; Li, F.; Chekhovich, E. A.; Borisenko, D. N.; Kolesnikov, N. N.; Novoselov, K. S.; Skolnick, M. S.; Smith, J. M.; Krizhanovskii, D. N.; Tartakovskii, A. I. Two-Dimensional Metal−Chalcogenide Films in Tunable Optical Microcavities. *Nano Lett.* **2014**, *14*, 7003−7008.
(55) Kim, J. C.; Wake, D. R.; Wolfe, J. P. Thermodynamics of Biexcitons in a GaAs Quantum Well. *Phys. Rev. B* **1994**, *50*, 15099.
(56) Rodt, S.; Heitz, R.; Schliwa, A.; Sellin, R. L.; Guffarth, F.; Bimberg, D. Repulsive Exciton-Exciton Interaction in Quantum Dots. *Phys. Rev. B* **2003**, *68*, No. 035331.
(57) Stier, O.; Schliwa, A.; Heitz, R.; Grundmann, M.; Bimberg, D. Stability of Biexcitons in Pyramidal Inas/Gaas Quantum Dots. *Phys. Status Solidi B* **2001**, *224*, 115−118.
(58) Stier, O. Theory of the Electronic and Optical Properties of Ingaas/Gaas Quantum Dots. In *Nano-Optoelectronics*; Springer, 2002; pp 167−202.
(59) Lelong, P.; Heller, O.; Bastard, G. Coulomb Interactions in Small InAs Quantum Dots. *Solid-State Electron.* **1998**, *42*, 1251−1256.
(60) Brooks, M.; Burkard, G. Theory of Strain-Induced Confinement in Transition Metal Dichalcogenide Monolayers. *Phys. Rev. B* **2018**, *97*, No. 195454.
(61) Carmesin, C.; Lorke, M.; Florian, M.; Erben, D.; Schulz, A.; Wehling, T. O.; Jahnke, F. Quantum-Dot-like States in Molybdenum Disulfide Nanostructures Due to the Interplay of Local Surface Wrinkling, Strain, and Dielectric Confinement. *Nano Lett.* **2019**, *19*, 3182−3186.
(62) Stier, O.; Grundmann, M.; Bimberg, D. Electronic and Optical Properties of Strained Quantum Dots Modeled by 8-Band K· p Theory. *Phys. Rev. B* **1999**, *59*, 5688.
(63) Benyoucef, M.; Yacob, M.; Reithmaier, J. P.; Kettler, J.; Michler, P. Telecom-Wavelength (1.5 μ m) Single-Photon Emission from InP-Based Quantum Dots. *Appl. Phys. Lett.* **2013**, *103*, 162101.
(64) He, Y.-M.; Iff, O.; Lundt, N.; Baumann, V.; Davanco, M.; Srinivasan, K.; Höfling, S.; Schneider, C. Cascaded Emission of Single Photons from the Biexciton in Monolayered WSe2. *Nat. Commun.* **2016**, *7*, 13409.
(65) Landau, L. D.; Lifshitz, E. M. *Course of Theoretical Physics*; Elsevier, 2013.
(66) Kern, J.; Niehues, I.; Tonndorf, P.; Schmidt, R.; Wigger, D.; Schneider, R.; Stiehm, T.; Michaelis de Vasconcellos, S.; Reiter, D. E.; Kuhn, T.; Bratschitsch, R. Nanoscale Positioning of Single-Photon Emitters in Atomically Thin WSe_2. *Adv. Mater.* **2016**, *28*, 7101−7105.
(67) Darlington, T. P.; Krayev, A.; Venkatesh, V.; Saxena, R.; Kysar, J. W.; Borys, N. J.; Jariwala, D.; Schuck, P. J. Facile and Quantitative Estimation of Strain in Nanobubbles with Arbitrary Symmetry in 2D Semiconductors Verified Using Hyperspectral Nano-Optical Imaging. *J. Chem. Phys.* **2020**, *153*, No. 024702.
(68) Kolesnichenko, P. V.; Zhang, Q.; Yun, T.; Zheng, C.; Fuhrer, M. S.; Davis, J. A. Disentangling the Effects of Doping, Strain and Disorder in Monolayer WS2 by Optical Spectroscopy. *2D Mater.* **2020**, *7*, No. 025008.
(69) Li, H.; Li, H.; Wang, X.; Nie, Y.; Liu, C.; Dai, Y.; Ling, J.; Ding, M.; Ling, X.; Xie, D.; Lu, N.; Wan, C.; Xiong, Q.; Xu, W. Spontaneous Polarity Flipping in a 2D Heterobilayer Induced by Fluctuating Interfacial Carrier Flows. *Nano Lett.* **2021**, *21*, 6773−6780.
(70) Ryu, B.; Wang, L.; Pu, H.; Chan, M. K. Y.; Chen, J. Understanding, Discovery, and Synthesis of 2D Materials Enabled by Machine Learning. *Chem. Soc. Rev.* **2022**, *51*, 1899−1925.
(71) Ataca, C.; Grossman, J. C.; Tongay, S. Enhancing Light Emission Efficiency without Color Change in Post-Transition Metal Chalcogenides. In *ECS Meeting Abstracts*; IOP Publishing, 2018; p 868.
(72) Wu, Y.; Fuh, H.-R.; Zhang, D.; Coileáin, C. Ó.; Xu, H.; Cho, J.; Choi, M.; Chun, B. S.; Jiang, X.; Abid, M.; Abid, M.; Liu, H.; Wang, J. J.; Shvets, I. V.; Chang, C. R.; Wu, H. C. Simultaneous Large Continuous Band Gap Tunability and Photoluminescence Enhancement in GaSe Nanosheets via Elastic Strain Engineering. *Nano Energy* **2017**, *32*, 157−164.
(73) Le Toullec, R.; Piccioli, N.; Mejatty, M.; Balkanski, M. Optical Constants Ofε-GaSe. *Nuovo Cim. B* **1977**, *38*, 159−167.
(74) Adachi, S.; Shindo, Y. Optical Constants of ε-GaSe. *J. Appl. Phys.* **1992**, *71*, 428−431.
(75) Feng, J.; Qian, X.; Huang, C.-W.; Li, J. Strain-Engineered Artificial Atom as a Broad-Spectrum Solar Energy Funnel. *Nat. Photonics* **2012**, *6*, 866.
(76) He, R.; Meunier, M.; Dong, Z.; Cai, H.; Gao, W.; Zuniga-Perez, J.; Liu, X. Interplay of Purcell Effect and Extraction Efficiency in CsPbBr3 Quantum Dots Coupled to Mie Resonators. *Nanoscale* **2023**, *15*, 1652−1660.
(77) Ishii, T.; Kambe, N. GaSe Single Crystal Growth by Iodine Vapor Transport. *J. Cryst. Growth* **1986**, *76*, 489−493.
(78) Patel, R. N.; Hopper, D. A.; Gusdorff, J. A.; Turiansky, M. E.; Huang, T.-Y.; Fishman, R. E.; Porat, B.; Van de Walle, C. G.; Bassett, L. C. Probing the Optical Dynamics of Quantum Emitters in Hexagonal Boron Nitride. *PRX Quantum* **2022**, *3*, No. 030331.
(79) Branny, A.; Kumar, S.; Proux, R.; Gerardot, B. D. Deterministic Strain-Induced Arrays of Quantum Emitters in a Two-Dimensional Semiconductor. *Nat. Commun.* **2017**, *8*, 15053.
(80) Perdew, J. P.; Burke, K.; Ernzerhof, M. Generalized Gradient Approximation Made Simple. *Phys. Rev. Lett.* **1996**, *77*, 3865.

https://doi.org/10.1021/acsphotonics.3c00052
ACS Photonics XXXX, XXX, XXX−XXX

(81) *Materials Data on GaSe by Materials Project*; mp-1572; Lawrence Berkeley National Lab. (LBNL), Berkeley, CA (United States). LBNL Materials Project, **2020**. 10.17188/1191339.

(82) Wang, V.; Xu, N.; Liu, J.-C.; Tang, G.; Geng, W.-T. VASPKIT: A User-Friendly Interface Facilitating High-Throughput Computing and Analysis Using VASP Code. *Comput. Phys. Commun.* **2021**, *267*, No. 108033.

https://doi.org/10.1021/acsphotonics.3c00052
ACS Photonics XXXX, XXX, XXX−XXX